



HAL
open science

PEGylated PNiPAM Microgels : Synthesis, Characterization and Colloidal Stability

Julien Es Sayed, Cédric Lorthioir, Patrick Perrin, Nicolas Sanson

► **To cite this version:**

Julien Es Sayed, Cédric Lorthioir, Patrick Perrin, Nicolas Sanson. PEGylated PNiPAM Microgels : Synthesis, Characterization and Colloidal Stability. *Soft Matter*, 2019, 15, pp.963-972. 10.1039/c8sm02156b . hal-01966786

HAL Id: hal-01966786

<https://hal.science/hal-01966786>

Submitted on 29 Dec 2018

HAL is a multi-disciplinary open access archive for the deposit and dissemination of scientific research documents, whether they are published or not. The documents may come from teaching and research institutions in France or abroad, or from public or private research centers.

L'archive ouverte pluridisciplinaire **HAL**, est destinée au dépôt et à la diffusion de documents scientifiques de niveau recherche, publiés ou non, émanant des établissements d'enseignement et de recherche français ou étrangers, des laboratoires publics ou privés.

1 PEGylated PNiPAM Microgels : Synthesis,
2 Characterization and Colloidal Stability

3 *Julien Es Sayed,^a Cédric Lorthioir,^b Patrick Perrin,^{a*} and Nicolas Sanson^{a*}*

4 ^a Soft Matter Sciences and Engineering, ESPCI Paris, PSL University, Sorbonne Université,
5 CNRS, F-75005 Paris.

6 ^b Sorbonne Université, CNRS, Collège de France, Laboratoire de Chimie de la Matière
7 Condensée de Paris, LCMCP, F-75005 Paris.

8

9

10

11

12

13

14

15

16

17 **ABSTRACT**

18 The challenge of this work is to synthesize highly stable thermoresponsive microgels that
19 could be used in diverse applications. To achieve this, *N*-isopropylacrylamide (NiPAM) based
20 microgels were first synthesized by surfactant-free precipitation polymerization of NiPAM in
21 the presence of poly(ethylene glycol) methacrylate (PEG) as macro-comonomer and
22 methylene-bis-acrylamide (MBA) as chemical crosslinker. By combining a complete set of
23 techniques such as dynamic light scattering (DLS), scanning electron microscopy (SEM),
24 zetametry, ¹H NMR and micro-differential scanning calorimetry (μDSC), we clearly
25 demonstrate that (i) the incorporation of the PEG chains control the size and the
26 polydispersity of the NiPAM-based microgels whereas the thermal behavior in solution
27 (enthalpy, volume phase transition temperature, VPTT) remains almost the same as for pure
28 NiPAM microgels (ii) the PEG chains are mainly located at the microgel periphery and (iii)
29 the presence of the PEG chains strongly increases the colloidal stability of microgels in
30 electrolyte solutions at high temperature.

31

32

33

34

35

36

37

38

39

40

41 INTRODUCTION

42 During the last three decades, nanogels/microgels have received considerable interest for
43 applications in diverse domains notably in biomedical applications such as drug delivery,
44 biosensors, targeted therapies, ¹⁻⁵... Microgels are defined as colloidal gel particles having
45 diameters in the range from 0.05 to 1 μm exhibiting network structure that swells in a suitable
46 solvent. Research has been directed towards the synthesis of *stimuli*-responsive or "*smart*"
47 microgels, which properties can be modulated reversibly in response to an environmental
48 *stimulus* such as pH, temperature, and light to name but a few.⁶ Among the *stimuli*-responsive
49 microgels, it is well established that thermoresponsive *N*-isopropylacrylamide (NiPAM) based
50 microgels are the most used mainly due to both the polymerization process which allow to
51 synthesize well-defined pure or functionalized particles and its volume phase transition
52 temperature close to human body.⁷ However, while the microgel synthesis is now well
53 described, the control of the colloidal stability of thermoresponsive microgels remains a key
54 challenge for their use in the applications cited previously.

55 Generally, for a dispersion of pure NiPAM microgels, an increase of electrolyte
56 concentration leads to (i) a decrease of the microgel size (ii) a shift of the VPTT towards
57 lower temperatures and (iii) an aggregation at temperatures higher than the VPTT.⁸⁻¹⁰ One of
58 the strategies to improve the colloidal stability of thermoresponsive microgels is to
59 incorporate suitable comonomers such as charged ones at the periphery of the microgel
60 network to maintain a sufficiently high hydrophilicity at high temperature, typically above the
61 so-called Volume Phase Transition Temperature (VPTT). For instance, Farooqi et al. showed
62 that microgels synthesized by copolymerizing NiPAM and different acrylic acid (AAc)
63 contents are colloiddally stable at pH 9 up to 0.1 M whatever the temperature. However, at pH
64 values higher than the pKa of acrylic acid, the VPTT shifts towards high temperature until it
65 disappears.¹¹ Moreover, decreasing pH leads to poly(NiPAM-*co*-AAc) microgels aggregation

66 at temperatures above the microgel VPTT in pure water. In order to tackle the VPTT
67 dependence of the poly(NiPAM-*co*-AAc) microgels towards pH, Das et al. have incorporated
68 sulfobetaine monomers into NiPAM-based microgels. Due to the high hydrophilicity of the
69 zwitterionic monomers, the colloidal stability was maintained up to 1 M NaCl even at high
70 temperatures. However, the incorporation of zwitterionic monomers into the microgel leads to
71 an increase of the microgel size as well as a shift of the VPTT towards high temperature.¹²
72 The colloidal stability of thermoresponsive NiPAM microgels can also be improved by
73 incorporation of poly(ethylene glycol) (PEG) chains, which are well known to shield the
74 surface of polymeric colloids against aggregation.¹³ This concept was used by Gan et al., who
75 first synthesized thermoresponsive microgels that efficiently resist protein adsorption-induced
76 aggregation. The authors prepared PEGylated thermoresponsive microgels by surfactant
77 precipitation polymerization by copolymerization of NiPAM with PEG macro-comonomers
78 ($M_w=1000$ g/mol).¹⁴ However, increasing PEG content (from 10 to 40 wt %) leads to
79 microgels with an increasing polydispersity with both a shift to higher temperature and a
80 broadness of the VPTT. Similar observations were made recently by Trongsalitkul et al. for
81 NiPAM microgels containing PEG chains with different number average molar masses M_n
82 ranging from 300 to 1100 g/mol.¹⁵
83 In the light of the reports cited above, it appears challenging to synthesize thermoresponsive
84 NiPAM-based microgels presenting a high colloidal stability without changing their solution
85 properties. To tackle this problem, we synthesized thermoresponsive NiPAM-based microgels
86 by surfactant-free precipitation copolymerization of NiPAM and poly(ethylene glycol)
87 methacrylate. Compared to previous reported works, we investigated in the present work how
88 to synthesize monodisperse PEGylated NiPAM-based microgels of different sizes with high
89 colloidal stability in electrolyte solution without changing the microgel VPTT.

91
92
93
94
95
96
97
98
99
100
101
102
103
104
105
106
107
108
109
110
111
112
113
114

EXPERIMENTAL

Materials

N-isopropylacrylamide (NiPAM) monomer, *N,N'*-methylenebisacrylamide (MBA) and potassium persulfate (KPS) were purchased from Sigma-Aldrich and used as received. Poly(ethylene glycol) monomethacrylate (PEGMAOH) macromonomer with a weight average molar mass of $M_w=2000$ g/mol was purchased from Polysciences. Ultrapure deionized water with a minimum resistivity of 18 M Ω .cm (milliQ, Millipore, France) was used all experiments.

Synthesis of Microgels

All NiPAM-based microgels were synthesized by surfactant-free precipitation polymerization.¹⁶ In a typical synthesis, 3 g of NiPAM (26.5 mmol) were dissolved in 210 mL of water in a three-neck round-bottom flask equipped with a condenser under stirring (250 rpm) with a teflon semi-lunar shaped stirring blade at ambient temperature and under N₂ flow. Pre-dissolved MBA in 40 mL of water (2 mol % vs NiPAM monomer) and PEGMAOH in 40 mL of water (from 0 to 1 mol % vs NiPAM monomer) were added to the reaction mixture. The reaction medium was then heated to 67 °C and purged under N₂ flow for 40 minutes. Subsequently, KPS previously dissolved in 10 mL of water (2 mol % vs NiPAM monomer), was injected in the reaction mixture and the reaction was allowed to progress for 4 hours under continuous stirring (250 rpm) and N₂ flow. Finally, the reaction media was exposed to

115 air and the flask was immersed in an ice-cold bath in order to stop the polymerization. The
 116 synthesized microgels were purified from un-reacted monomers and free polymer chains by
 117 extensive dialysis (Spectra/Por dialysis membrane, MWCO 10^6 Da) against water for 2 weeks
 118 until the value of supernatant surface tension was equal to that of pure water, 70 mN/m at 20
 119 °C therefore ensuring high-quality purification of the microgels. After purification, the
 120 microgels were freeze-dried. The composition of the reaction mixture of the microgels are
 121 gathered in Table 1. They are noted MG-X where X is the PEGMAOH macromonomer to
 122 NiPAM feed monomer molar ratio.

123

124 **Table 1** Chemical composition of PEGylated NiPAM microgels

<i>Microgels</i>	<i>NiPAM</i>	<i>MBA</i>	<i>KPS</i>	<i>PEGMAOH^a</i>	<i>PEGMAOH^b</i>	<i>PEGMAOH^c</i>
	n (mmol)	mol %	mol %	mol %	mol %	wt %
MG-0	26.5	2	2	0	0	0
MG-0.1	26.5	2	2	0.1	0.09	1.3
MG-0.25	26.5	2	2	0.25	0.18	3.2
MG-0.5	26.5	2	2	0.5	0.36	6.0
MG-1	26.5	2	2	1	0.74	11.7

125 ^a Feed ratio of PEG macromonomer to NiPAM monomer used in the microgel synthesis. ^{b,c} Molar and
 126 weight ratios of PEG macromonomer to NiPAM within the microgel, determined by ¹H NMR.

127

128 **Characterization**

129 ¹H NMR. NMR experiments in deuterated DMSO were performed on a Bruker Avance III
 130 HD spectrometer operating at 400 MHz for ¹H, using a standard 5 mm broadband Smart
 131 probe at 25 °C.

132 ^1H solution-state NMR measurements were conducted on a Bruker Avance 300 NMR
133 spectrometer at a magnetic field of 7.0 T, corresponding to a ^1H Larmor frequency of 300.1
134 MHz. Variable-temperature single-pulse experiments between 2 and 70 °C were performed
135 using a 5 mm inverse $^1\text{H}/^{13}\text{C}$ -selective probe and a BCU accessory, for the temperature range
136 from 2 to 25 °C. The 90° pulse length was set to 7.5 μs and the recycle delay was adjusted to
137 at least 5 times the longest T_1 (^1H) relaxation time, i.e. between 30 and 90 s, depending on the
138 temperature value. The ^1H transverse relaxation signal was determined using the PROJECT
139 pulse sequence (*Periodic Refocusing Of J Evolution by Coherence Transfer*)¹⁷, with a value of
140 the interpulse delay, τ , set to 0.25 ms. The measured relaxation functions were normalized by
141 the amplitude of the ^1H magnetization following a single cycle of the PROJECT experiment
142 (that is to say [τ -180°- τ -90°- τ -180°- τ]).

143 The quantification of the concentration of EG and NiPAM repeat units as a function of
144 temperature was obtained by means of a solution of maleic acid in D_2O , chosen as an external
145 reference. A 5 mm tube with a coaxial insert (NI5CCI-B, Norell) filled by such a solution,
146 prepared with an accurately-defined concentration (22.1 mM), was systematically used for all
147 the investigated microgel solutions. Prior to the experiments, a calibration of the temperature
148 probe was carried out using a solution of ethylene glycol in deuterated DMSO (concentration
149 of 80 wt %) with the same coaxial insert containing the above-described solution of maleic
150 acid in D_2O . Following each temperature change and once the target value was achieved for at
151 least 10 s, a delay of 15 min was introduced in order to ensure the thermal equilibration of the
152 sample. During the NMR measurements, the temperature was regulated within ± 1 °C.

153 *Dynamic light scattering (DLS)*. Dynamic light scattering was performed on an ALV
154 goniometer (ALV/CGS-3) with a He/Ne laser operated at a wavelength of $\lambda = 633$ nm, in
155 combination with an ALV/LSE-5003 correlator. Prior to DLS measurements, all samples
156 were prepared with ultrapure water (Milli-Q, Millipore, France) at a microgel concentration

157 $C_{MG} = 0.01$ wt %. The microgel solutions were equilibrated overnight at room temperature,
158 and filtered through Nylon filters of $0.8 \mu\text{m}$ pore size. In order to study the variation of the
159 size of the microgel as a function of temperature, the samples were kept at rest within the
160 apparatus at each temperature for 10 min prior to measurements. The results are given as
161 intensity-averaged hydrodynamic diameters (mean diameters based on the intensity of the
162 scattered light).

163 *Scanning electron microscopy (SEM).* Scanning electron microscopy observations were
164 performed on a FEG Magellan 400 FEI Thermofisher microscope. The observation takes
165 place at a high acceleration tension of 5 kV.

166 *Micro-calorimetry (μDSC).* The phase transition of NiPAM-based microgels in aqueous
167 solution was investigated by Micro Differential Scanning Calorimetry using a micro DSC III
168 instrument from SETARAM. The microgel solution ($C_{MG} = 0.5$ wt %) and the reference filled
169 with the same quantity of solvent, were equilibrated and submitted to a temperature cycle
170 between 10 and 50 °C. Both heating and cooling rates were fixed at 0.1 °C/min.

171 *Zeta-potential measurements.* The zeta-potential (ζ) of the synthesized microgels was
172 determined from 15 to 50 °C by a Zetasizer Nano-ZS90 from Malvern. Microgels were
173 suspended in a 10^{-4} M NaCl water solution at a concentration of $C_{MG} = 0.1$ wt % and the
174 solutions were left 10 min at each temperature prior to measurements.

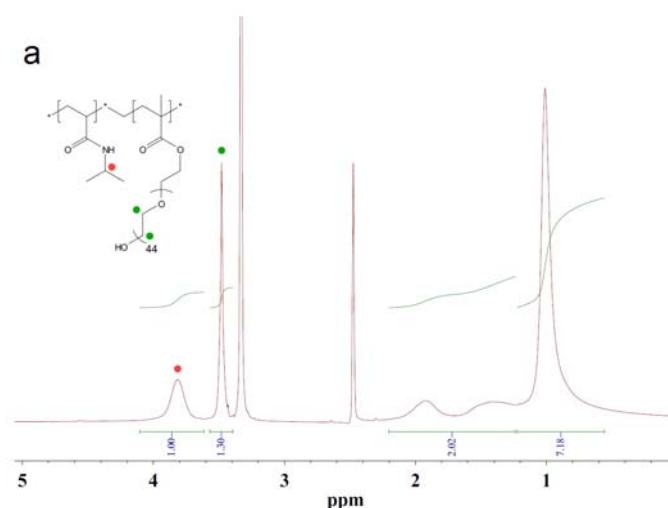
175

176 **RESULTS AND DISCUSSION**

177 Several microgels were synthesized by surfactant free copolymerization of *N*-
178 isopropylacrylamide (NiPAM) as main monomer and different amounts of poly(ethylene
179 glycol) monomethacrylate (PEGMAOH) as co-monomer from 0 to 1 mol % corresponding to
180 a maximum weight ratio of 11.7 wt % as reported in **Table 1**. The chemical compositions of
181 the NiPAM-based microgels have been investigated using ^1H NMR spectroscopy in

182 deuterated DMSO- d_6 as shown in **Figure 1**. The amount of PEG macromonomer incorporated
183 within the microgel was determined by comparing the peak areas assigned to the methylene
184 protons of the PEG macro-comonomer (3.5 ppm) and one related to the isopropyl group of
185 NiPAM (3.8 ppm) (**Figure 1a**). **Figure 1b** shows the molar ratio of PEG macromonomer to
186 NiPAM within the microgel as a function of the molar ratio of PEG macromonomer to
187 NiPAM introduced in the batch synthesis. The linear variation indicates that the molar ratio of
188 PEG macromonomer to NiPAM units within all the synthesized microgels is equal to 74 %
189 irrespective of the feed molar ratio of PEG macromonomer to NiPAM. Knowing that the PEG
190 macromonomer content introduced in the reaction medium is low, the value of the
191 incorporation rate of PEG macromonomer into the microgel is in line with the theoretical
192 value according the reactivity ratios, $r_{\text{NiPAM}}=1.2$ and $r_{\text{PEGMAOH}}=0.13$ reported by Alava et al.¹⁸
193 In order to investigate the influence of PEG incorporation on the size, polydispersity,
194 swelling ratio, volume phase transition temperature and transition enthalpy of NiPAM-based
195 microgels, they were characterized by combining dynamic light scattering (DLS), scanning
196 electron microscopy (SEM), proton NMR spectroscopy and microcalorimetry.

197



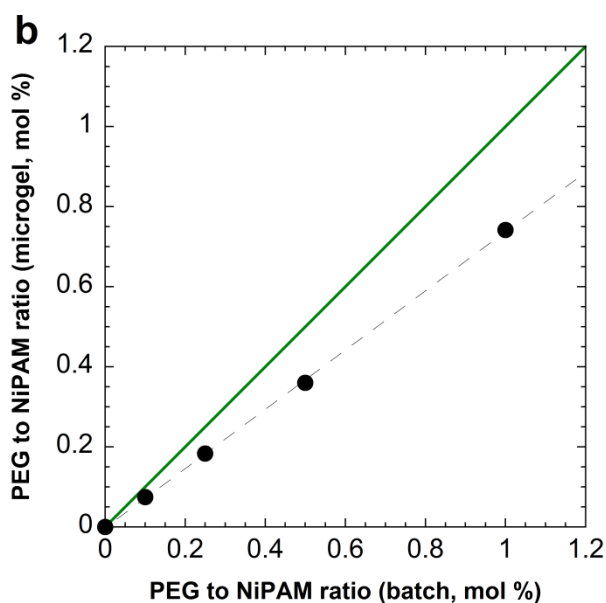


Fig. 1 (a) ^1H NMR spectrum of MG-1 in DMSO-d_6 at $25\text{ }^\circ\text{C}$ and corresponding chemical structure. **(b)** Efficiency of the PEG macromonomer incorporation in the NiPAM-based microgel. Correlation between the microgel composition (mol %) and the batch synthesis ratio of PEG chains to NiPAM repeat units. The PEG to NiPAM molar ratios have been determined by ^1H NMR. The solid line (green) represents a theoretical 100% incorporation efficiency.

198

199 ***Influence of PEG incorporation on the NiPAM phase separation process***

200 As NiPAM is the main component of the synthesized microgels, we first investigated their
 201 thermosensitive character using micro-calorimetry since the transition temperature as well as
 202 the transition enthalpy are coupled to the structure of the polymer chain (chemical
 203 composition, architecture) and to the environmental conditions (co-solvent, ionic strength). A
 204 typical thermogram carried out at a slow rate of $0.1\text{ }^\circ\text{C}/\text{min}$ in order to minimize the kinetic
 205 effects is given in **Figure 2a** for MG-1, the microgel with a PEG batch concentration of 1 mol
 206 % corresponding to 11.7 wt %. The microgels exhibit a heating endothermic peak and cooling
 207 exothermic peak characteristic of the thermal phase transition of NiPAM polymer chains
 208 embedded into the microgel. This endothermic process observed during the heating scan is
 209 related to the overall energy balance of hydrogen bonds disruption/reformation between

210 amide groups and water molecules.¹⁹ For the different microgels, both the thermal enthalpy,
211 ΔH , expressed in kJ per mole of NiPAM and peak temperature, T_{peak} , respectively
212 corresponding to the area under the thermogram and the temperature where the thermal
213 capacity is the highest were plotted as a function of the PEG macromonomer to NiPAM
214 monomer molar ratio (**Figure 2b**). Note that the obtained values were normalized by the real
215 amount of NiPAM repeat units into the microgel determined by ¹H NMR spectroscopy. The
216 pure NiPAM microgels, MG-0, shows the highest enthalpy with a value of $\Delta H=5.3$ kJ/mol
217 consistent with reported studies.^{20, 21} The enthalpy of NiPAM-based microgels, in which PEG
218 macromonomers have been incorporated, decreases with increasing the PEG macromonomer
219 content from 4.9 kJ/mol for MG-0.25 to 4 kJ/mol for MG-1 while the peak temperature
220 remains unchanged. A reasonable explanation would be that the grafted PEG chains hinder
221 the phase separation process of NiPAM polymer chains and consequently influence the values
222 of the transition enthalpy. This was shown by Chen et al. by studying four poly(NiPAM)
223 grafted poly(ethylene oxide) of almost the same average molar mass, PNiPAM-*g*-PEO
224 copolymers, with different NiPAM/PEO molar ratio. They observed that the phase transition
225 enthalpy of the copolymers decreases from 5.6 kJ/mol for the higher NiPAM/PEO ratio to 1.7
226 kJ/mol for the copolymers having the lower NiPAM/POE ratio, i.e. the copolymers with the
227 higher PEO content.²² On their side, Spevacek et al. also reported that the architecture of the
228 copolymers strongly impacts the phase transition enthalpy of the NiPAM-based copolymers.
229 They demonstrate a sharp decrease of the enthalpy value for diblock copolymers, PEO-*b*-
230 PNiPAM, and Y-shape triblock, PEO-*b*-(PNiPAM)₂, compared to NiPAM homopolymers.²³
231 Similarly, Lin et al. have shown that the transition enthalpy of copolymers constituted of PEG
232 and PNiPAM is impacted by the copolymers architecture (block or star).²⁴ In the present
233 work, we note that the phase transition temperature does not vary with the incorporation of
234 PEG within the microgels. This statement is not consistent with Teodorescu et al. who have

235 studied the phase transition of PNiPAM-*b*-PEG-*b*-PNiPAM triblock copolymers and observed
 236 that the phase transition temperature increases when decreasing the NiPAM to PEG ratio.^{25, 26}
 237
 238
 239
 240
 241

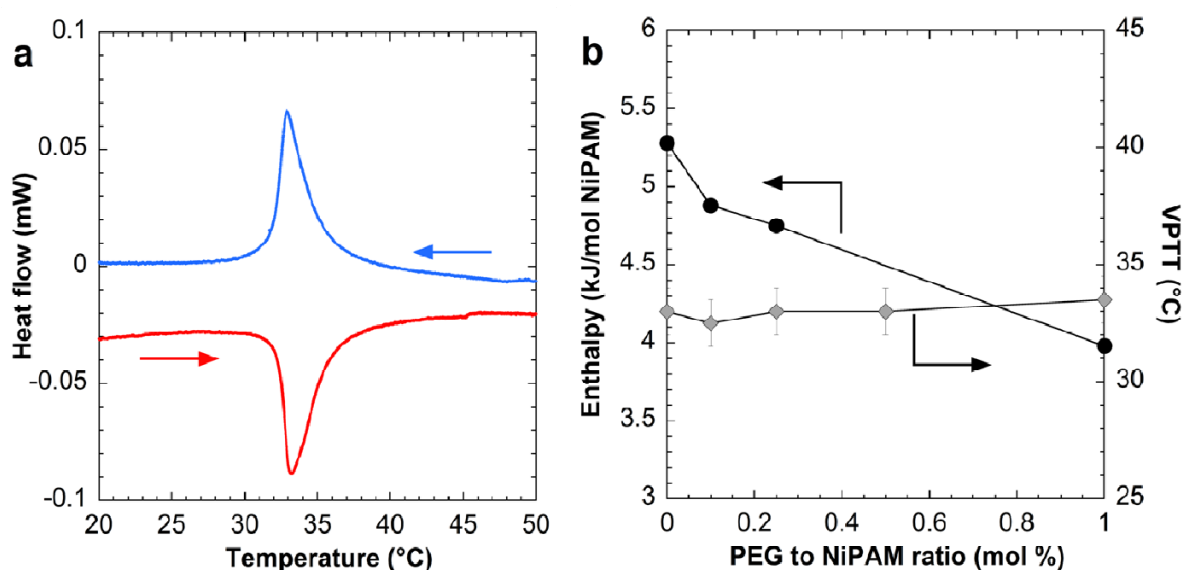


Fig. 2 (a) Thermograms of the MG-1 microgel obtained by μ DSC with a microgel concentration $C_{MG} = 0.5$ wt % at a heating and cooling rate of 0.1 °C/min. (b) Variation of the enthalpy (\bullet kJ/mol NiPAM) and VPTT (\blacklozenge) of PEGylated NiPAM-based microgels as a function of the PEG to NiPAM ratio.

242

243

244 *Influence of PEG incorporation on size, size polydispersity and VPTT of microgels*

245 The temperature dependence of the size of NiPAM-based microgels as a function of the
 246 PEG content was investigated using dynamic light scattering from 10 to 50 °C, i.e., at
 247 temperatures well below and above the temperature of the NiPAM phase transition previously
 248 determined by calorimetry (**Figure 2**). **Table 2** reports the main characteristics of the

249 microgels, namely their size, polydispersity, VPTT and estimated molar masses. Microgels
250 were also characterized by scanning electron microscopy (SEM) (**Figure 4**). First, we can
251 observe in **Figure 3a** that both the temperature (33 ± 1 °C) and sharpness of volume phase
252 transition of NiPAM-based microgels are maintained whatever the amount of incorporated
253 PEG up to 11.7 wt % (MG1). These results are in contrast with reported studies where the
254 VPTT of NiPAM microgels shifts towards high temperature and becomes broader when
255 increasing the PEG macrocomonomer content in the NiPAM-based microgel due to the
256 hydrophilic character of PEG chains.^{14, 15, 27} This trend is indeed general as it was also
257 observed in the case of NiPAM microgels copolymerized with hydrophilic comonomers,
258 neutral or charged.^{12, 28, 29} Also, compared to pure NiPAM microgels (MG-0), PEGylated
259 PNiPAM-based microgels synthesized in the present work are monodisperse irrespective of
260 the PEG content as shown by SEM (**Figure 4**), in agreement with polydispersity indexes
261 (PDI= 0.03-0.09) obtained by dynamic light scattering (**Table 2**). Differences (size control
262 and VPTT) between reported studies on PEGylated NiPAM microgels^{14, 27} and our
263 synthesized microgels may be explained by both the polymerization process and the average
264 molar mass of the PEG comonomer. Gan et al. synthesized NiPAM microgels with PEG
265 methacrylate ($M_w=1000$ g/mol) by precipitation polymerization using sodium dodecyl sulfate
266 as surfactant. The use of surfactant, which controls the microgel growth,^{30, 31} allows them to
267 maintain a similar microgel size whatever the PEG macromonomer content which does not
268 participate to the microgel stabilization during the growth process. Surfactant precipitation
269 polymerization results to a higher incorporation of PEG into the microgel and consequently
270 changes the behavior in solution of the microgels, i.e. a shift of the VPTT towards high
271 temperature with PEG increasing. On the other hand, Ma et al. have synthesized NiPAM
272 microgels by surfactant free precipitation polymerization using low molar mass PEG
273 methacrylate ($M_n =520$ g/mol). The incorporation of the PEG of low molar mass has almost

274 no effect on the microgel final size (from $R_h = 230$ to 250 nm) in spite of the PEG amount
275 used in the synthesis (from 0 to 8 mol % respectively). However, this incorporation strongly
276 impacts the VPTT of the microgels which shifts towards high temperature. Finally, the
277 comparison of both the characteristics of the microgels (size, polydispersity) and their thermal
278 behavior (VPTT) between reported studies and the present work is not straightforward.
279 Furthermore, Pich et al. who synthesized poly(*N*-vinyl caprolactam) microgels with a PEG
280 methacrylate similar to the one we have used ($M_w = 2000$ g/mol) which exhibit a similar
281 behavior concerning the evolution of the size of the microgel as a function of the PEG
282 methacrylate content, i. e., the microgel size decreases as the PEG amount in the synthesis
283 increases.³² In our case, the value and the sharpness of the VPTT of the microgels remains
284 unchanged whatever the PEGMAOH introduced in the reaction medium. Based on the
285 reactivity ratios of both monomers reported by Alava et al., this assumes that synthesized
286 microgels exhibit a structure where the NiPAM monomers mainly constitute the core and
287 PEG chains are located on the microgel periphery. Due to this composition, PEG chains do
288 not disrupt the phase transition of PNiPAM chains and consequently the VPTT of the
289 microgels. This hypothesis is supported by the research work of Hoare et al. on the synthesis
290 of NiPAM-based microgels with acid comonomers with different reactivity ratios. More
291 precisely, they observe that the VPTT of microgels do not change when the comonomers,
292 according to the reactivity ratios, are located at the microgel periphery.³³

293 **Figure 3b** shows that the size of the microgel linearly decreases from a hydrodynamic
294 radius value, R_h , around 330 nm (MG-0) to 110 nm (MG-1) at 25 °C when increasing PEG
295 molar ratio from 0 to 1 mol %. The evolution of the microgel size with the PEG
296 macromonomer content can reasonably be explained by considering their polymerization
297 mechanism. It is generally well accepted that microgels grow until they acquire a colloidal
298 stability, which prevents the addition of either free chains or other precursor particles. For the

299 pure NiPAM microgel, MG-0, the colloidal stability is only achieved owing to electrostatic
300 repulsions coming from the presence of the charged initiator. In the case of PEGylated
301 NiPAM microgels, the presence of PEG chains, which remain in good solvent at 67 °C
302 provides microgels with a supplementary stability of steric origin in addition to the
303 electrostatic stabilization due to the initiator. Consequently, the growth of the microgels may
304 stop at an earlier stage. As a result, the higher the PEG ratio, the smaller the microgel size.

305 The microgel swelling ratios, Q_v defined as the quotient of the hydrodynamic volumes at 25
306 °C and 45 °C are reported in **Table 2**. We found that the swelling ratios of all the PEG
307 containing microgels are around an average value of 10 whereas the swelling ratio of MG-0 is
308 about 20. For pure NiPAM microgels synthesized by surfactant free precipitation
309 polymerization, it is well-known that microgels exhibit a non uniform morphology induced by
310 a radial distribution of the crosslink points in the microgel network due to the reactivity
311 difference between the crosslinker, MBA, and NiPAM. Indeed, it has been reported that the
312 conversion rate of MBA is faster than NiPAM monomer leading to the presence of PNiPAM
313 dangling chains, formed at the end of the reaction, at the microgel periphery.^{34, 35} The
314 presence of the dangling chains, which extend towards the aqueous phase strongly impacts on
315 the hydrodynamic diameter at temperatures below the microgel's VPTT. However, at
316 temperatures higher than VPTT, the collapse of both the PNiPAM dangling chains and
317 microgel core leads to high values of the swelling ratio Q_v . In our case, we assume that the
318 rapid incorporation of the PEG chains into the microgel, which stops their growth earlier in
319 the polymerization process, decreases the number of PNiPAM dangling chains at the
320 periphery of the microgel. As a consequence, the difference in size between the swollen and
321 collapsed states of the microgels below and above VPTT is of a lesser importance therefore
322 inducing smaller Q_v swelling ratios.

323 We would like to point out that the synthesis of PEGylated microgels is highly
324 reproducible. Indeed, different synthesis batches give microgels with similar sizes and
325 temperature dependences as the size of the symbols represents the microgel size error
326 bars.(**Figure S1** in Supporting Information, SI).
327

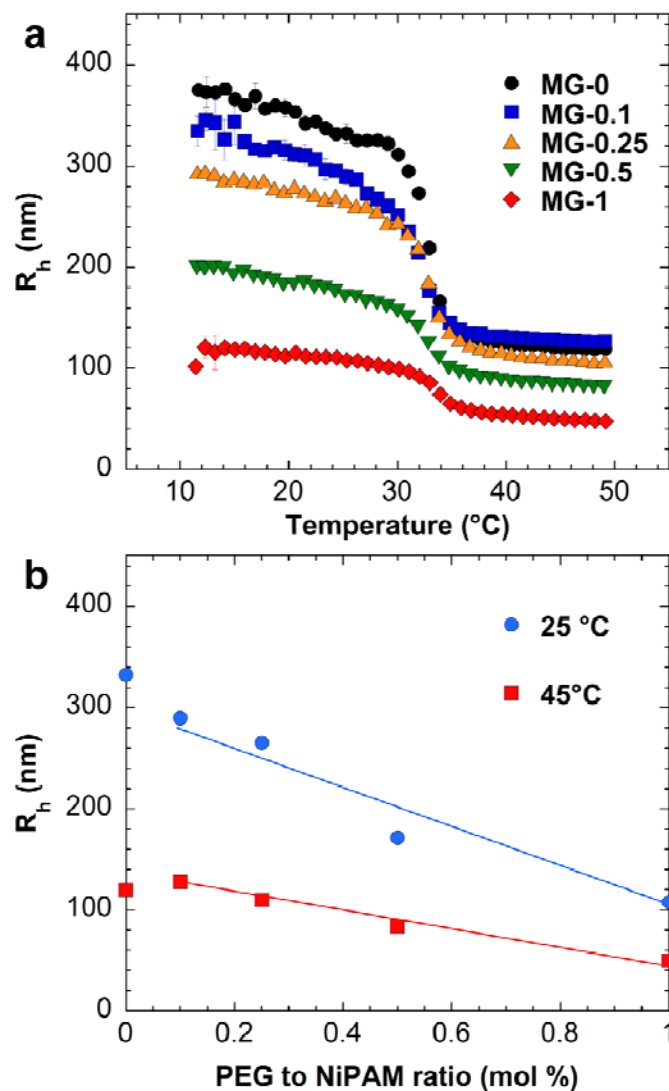


Fig. 3 (a) Hydrodynamic radius, R_h , of the PEGylated NiPAM-based microgels as a function of temperature. **(b)** Hydrodynamic radius, R_h , of the PEGylated microgels at 25 and 45 °C as a function of the molar ratio of PEGMAOH to NiPAM in the batch synthesis. The lines are guides for the eyes.

328

329

330

331

332

333

334

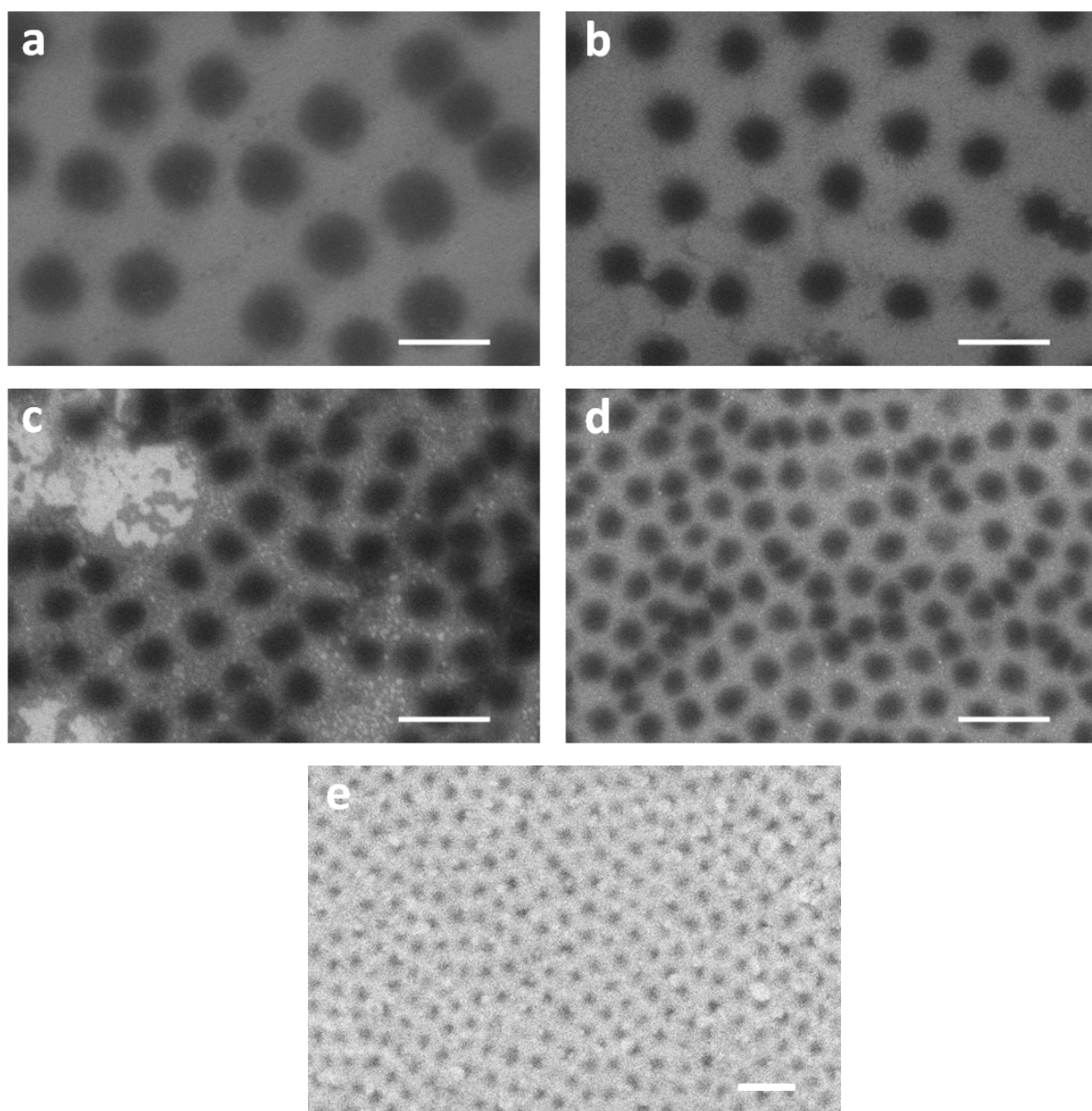


Fig. 4 SEM images of PEGylated microgels (a) MG-0, (b) MG-0.1, (c) MG-0.25, (d) MG-0.5 and (e) MG-1. The scale bar is 1 μm.

335

336 **Table 2** Hydrodynamic radius, polydispersity, swelling ratio, VPTT and estimated molar
 337 mass of the synthesized microgels deduced from DLS measurements

<i>Microgel</i>	$R_h (25\text{ }^\circ\text{C})$ (nm)	$PDI (25\text{ }^\circ\text{C})$	$R_h (45\text{ }^\circ\text{C})$ (nm)	$PDI (45\text{ }^\circ\text{C})$	Q_v^a	$VPTT$ ($^\circ\text{C}$)	$M_w 10^6$ (g/mol) ^b
MG-0	332	0.22	119	0.03	21 ± 1	33	3435
MG-0.1	289	0.06	127	0.01	11 ± 1	33	4131
MG-0.25	265	0.09	110	0.03	14 ± 1	33	2621
MG-0.5	171	0.03	83	0.02	9 ± 1	33	1163
MG-1	107	0.08	49	0.02	10 ± 1	33	242

338 ^a The swelling ratio Q_v was defined as follows $Q_v = R_h (25\text{ }^\circ\text{C}) / R_h (45\text{ }^\circ\text{C})$ ^b The molar mass of the microgel was

339 estimated from the equation $n = \frac{3mass}{4(R_h (45\text{ }^\circ\text{C}))^3} \left(\frac{1}{\rho_{NiPAM}} + \frac{0.3}{0.7\rho_{water}} \right)$ (Lele et al., *Macromolecules* 1997, 30, 157)

340

341

342

343

344

345

346 ***Influence of PEG incorporation on the colloidal stability of NiPAM-based microgels***

347 As discussed in the introduction, the colloidal stability of stimuli-responsive microgels is

348 crucial for their use in many applications. In order to investigate the influence of the PEG

349 chains incorporation on the colloidal stability of PEGylated NiPAM-based microgels, we

350 studied the macroscopic stability diagrams and measured the zeta potential of the microgels.

351 The results are shown in **Figures 5** and **6**. The temperature dependence of the zeta potential,

352 ζ , for all synthesized microgels is characteristic of the general trend of thermoresponsive

353 NiPAM-based microgels synthesized using an anionic initiator.³⁶ First, at low temperature

354 microgels exhibit a low value of zeta potential coming from the dispersion of charges onto the

355 large microgel surface. Then, the absolute value of zeta potential rapidly increases above the

356 VPTT of the microgels, as the microgel collapses. As shown in **Figure 5**, we observe a clear
357 dependence of the zeta potential above the VPTT as PEG chains are incorporated into the
358 microgel. For instance, the absolute value of zeta potential decreases at 45 °C from $\zeta=-48$ mV
359 for pure NiPAM microgel (MG-0) to $\zeta=-16$ mV for microgel synthesized with 1 mol % of
360 PEG (MG-1). This feature may also be rationalized by considering the polymerization
361 mechanism of the microgels in the presence of PEG macro-comonomers. As already
362 discussed above, PEG chains provide additional stability during the polymerization process
363 and allow to stop earlier the growth of the microgel. As a consequence, we suggest that the
364 number of anionic sulfate groups within the microgel coming from the initiator decreases with
365 increasing the amount of PEG chains. This is coherent with the observed increase of the zeta
366 potential values for PEGylated microgels containing larger amount of PEG as temperature
367 exceeds VPTT.

368 However, a small amount of charges at the microgel surface is unfavorable to colloidal
369 stability, notably in the presence of electrolytes, which limits the range of applications. In
370 order to investigate the colloidal behavior of the microgels in aqueous solution, stability
371 diagrams were determined at various temperatures in the presence of a divalent salt (CaCl_2).
372 The results are shown in **Figure 6** and **Figure S2** in Supporting Information. It is widely
373 reported in the literature that the presence of electrolyte in microgel dispersions leads to a
374 temperature-induced flocculation characterized by a critical flocculation temperature.^{8, 10, 36, 37}
375 These reports converge to the fact that the higher the electrolyte concentration, the lower the
376 critical flocculation temperature. This general trend is verified in our case for pure NiPAM
377 microgel (MG-0) in the presence of calcium chloride with an aggregation of the microgels
378 observed from 0.01 M in CaCl_2 starting at 35 °C (**Figure 6a**) We also observed that the
379 critical flocculation temperature decreases when increasing the salt concentration.⁸
380 Remarkably, microgels synthesized with 1 mol % of PEG macro-comonomer (MG-1) are

381 stable over the whole range of investigated salt concentrations (up to 0.5 M CaCl₂) and
382 temperatures (up to 45 °C) (**Figure 6b**) except for the 1M CaCl₂ concentration for which the
383 aggregation starts above 35 °C. The colloidal stability of the microgels progressively
384 increases with the PEG content as shown in **Figure S2** in Supporting Information SI. These
385 results, which clearly demonstrate the efficiency of the PEG chains on the colloidal stability
386 of the microgels above VPTT strongly suggest that the PEG chains are located at the microgel
387 surface and protect them against aggregation. In order to investigate the localization of the
388 PEG moieties, NMR experiments were conducted as a function of temperature.
389

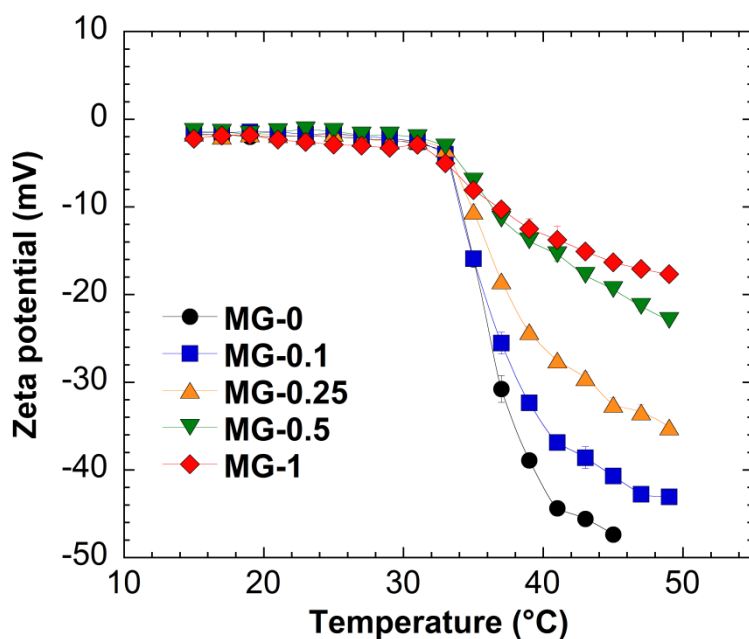


Fig. 5 Zeta potential as a function of the temperature for PEGylated microgel dispersions at a microgel concentration $C_{MG} = 0.1$ wt % in aqueous 10^{-4} M NaCl. The lines are guides to the eye.

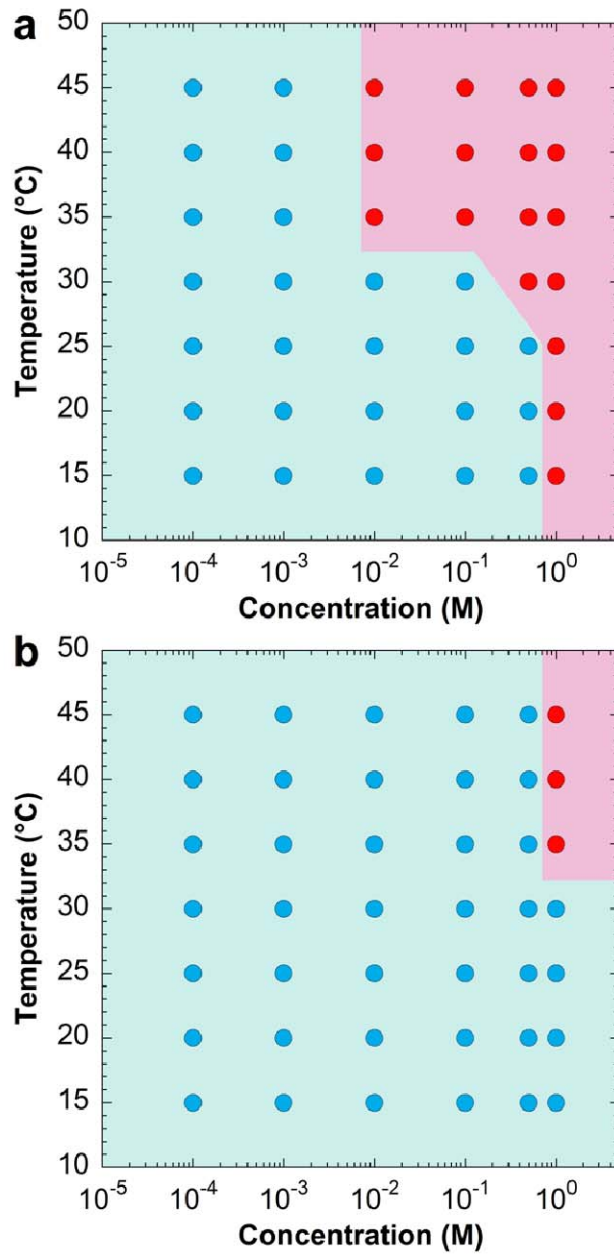


Fig. 6 Macroscopic stability diagrams of solutions of microgels (a) MG-0 and (b) MG-1, as a function of both the temperature and CaCl_2 concentration. The microgel concentration is $C_{\text{MG}} = 0.1$ wt %. The blue and red colors correspond to one and two phases respectively.

391 ***Localization of the PEG chains in the microgel network***

392 The evolution of the ^1H NMR spectrum obtained for MG-1 in D_2O was monitored using
393 isothermal steps during a heating ramp from 2 to 59 $^\circ\text{C}$, as described earlier in the
394 Experimental Section. **Figure 7a** shows the spectra recorded below and above the PNiPAM
395 VPTT. As expected, above the VPTT, the peaks related to the NiPAM units display a
396 significant broadening, resulting from the reduction of the segmental mobility along the
397 copolymer chains induced by the microgel contraction. Therefore, the signals from the
398 protons of the copolymer backbone (CH_2 and CH) and the methine proton of isopropyl group
399 ($\text{CH}(\text{CH}_3)_2$) are not detected any longer. The peak corresponding to the NiPAM CH_3 groups,
400 though broadened, is still observed, owing to their fast internal rotation around the C_3 axis.
401 Interestingly, above the VPTT, the peak related to the protons from the PEG side chains still
402 displays a relatively narrow contribution (about 5 Hz at 53 $^\circ\text{C}$). This result indicates that at
403 least part of the PEG repeat units (EG) is mobile enough to be observed, despite the microgel
404 collapse. Here, and in the following, the term "mobile" (or, respectively, "immobile" /
405 "frozen") refers to the segmental dynamics, probed over the tens of microseconds time scale.

406 In order to determine whether at least a fraction of the EG units gets frozen or not during the
407 heating ramp, the fraction of mobile EG units (f_{EG}) was measured as a function of
408 temperature, as shown in **Figure 7b**. The fraction of mobile NiPAM units (f_{NiPAM}) was also
409 included, for the sake of comparison. f_{NiPAM} was derived by considering the peak related to the
410 methine proton of the NiPAM isopropyl groups. Similar results were obtained using the peak
411 assigned to the protons of the NiPAM methyl groups (**Figure S3**, Supporting Information).
412 As expected, a significant and sharp decrease of f_{NiPAM} is observed above 38 $^\circ\text{C}$ and less than
413 7 % of the NiPAM units are detected then. These latter may partly correspond to low-
414 molecular-weight species.³⁸ The sharpness of the temperature evolution of f_{NiPAM} is in

415 agreement with the sharpness of $R_h(T)$, reported in **Figure 3a**. As far as the PEG side chains
 416 are concerned, the NMR experiments show that despite a concomitant decrease of f_{EG} above
 417 the VPTT, the fraction of the remaining mobile EG units is found to be quite significant,
 418 about 80 % for MG-1 for instance. This result indicates that only a relatively weak fraction of
 419 the EG units gets strongly slowed-down above the VPTT.

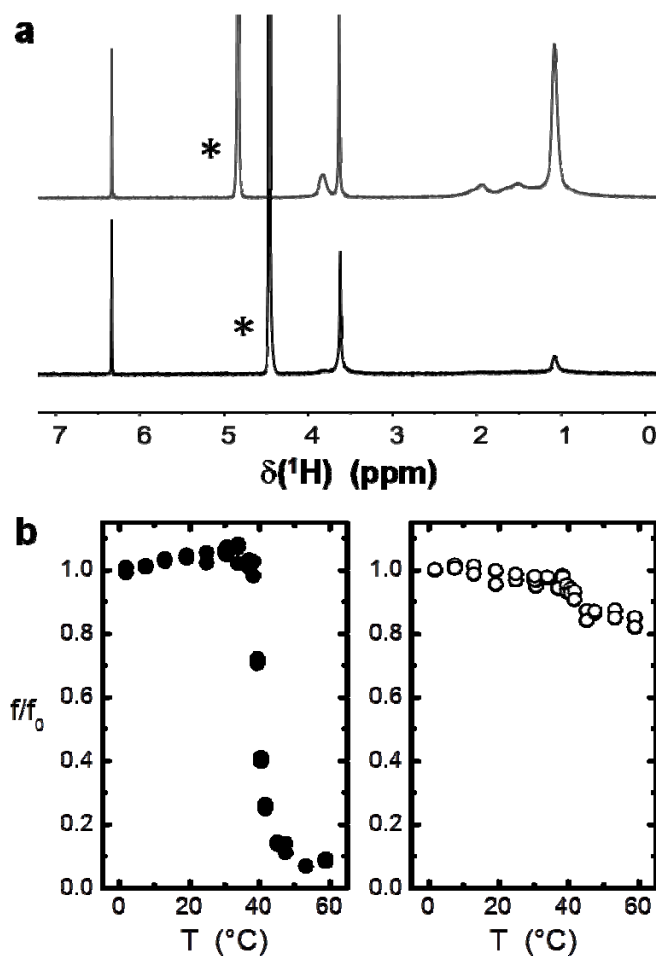


Fig. 7 (a) ^1H NMR spectra of MG-1 in D_2O at 19 and 53 $^\circ\text{C}$, respectively. The microgel concentration C_{MG} amounts to 0.05 wt %. The asterisk denotes the peak related to the residual protons of D_2O whereas the peak at 6.3 ppm corresponds to the CH protons of maleic acid. **(b)** Temperature dependence of the fraction f of mobile NiPAM (\bullet) and EG (\circ) units for MG-1 in D_2O . f_0 stands for the value of f at the lowest temperature considered (about 2 $^\circ\text{C}$).

421 The NMR measurements indicate that above the microgel VPTT, the segmental motions of
422 part of the PEG units remain fast over the tens of microseconds time scale. In this temperature
423 range, the preferential NiPAM/NiPAM interactions lead to the formation of hydrophobic
424 phase-separated NiPAM-rich globules and the hydrophilic PEG chains should tend to be
425 preferentially located out of the globules, that is to say at the outer part of the microgel
426 particles. From a dynamical point of view, such chains should experience a gradient of the
427 segmental mobility, with a progressive release of the local constraint from the external part of
428 the NiPAM-rich core toward the free end of the PEG chain. **Figure 8** depicts the ^1H
429 transverse relaxation signal determined for the EG units of MG-0.5, at 53 °C, that is to say
430 above the VPTT. In contrast to the situation observed below the VPTT (**Figure S4**,
431 Supporting Information), a clear deviation from a mono-exponential behavior is indeed
432 observed, which evidences the occurrence of a distribution of the segmental mobility along
433 the PEG chains. From a phenomenological point of view, this relaxation function may be
434 described using the sum of two exponential components, $A_s \times \exp(-t/T_{2s}) + A_L \times \exp(-t/T_{2L})$, with
435 $A_s = 66\%$ ($A_L = 33\%$), $T_{2s} = 70$ ms and $T_{2L} = 780$ ms. The fast relaxing component may be
436 assigned to the EG units displaying constrained segmental motions, due to the proximity with
437 the NiPAM-rich globules, whereas the long relaxation component should correspond to the
438 units located further from the core. At this stage, it should be noted that such a two-phase
439 model is a rough description of the continuous distribution of the local constraint occurring
440 along the PEG side chains.

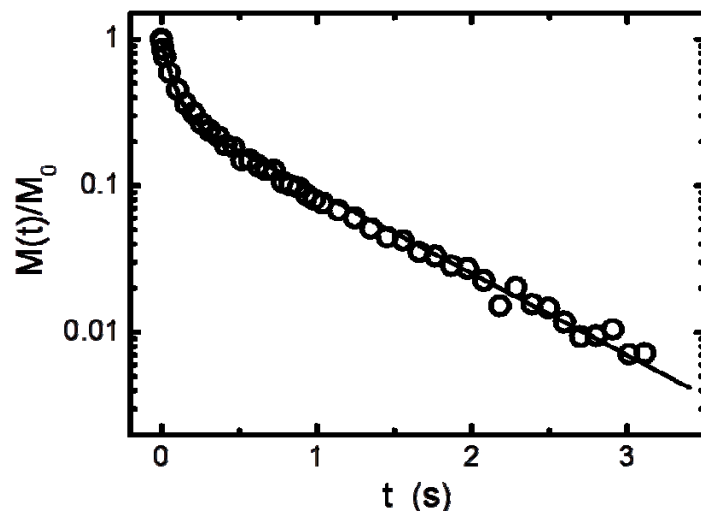


Fig. 8 ^1H transverse relaxation signal $M(t)$ for the protons of the PEG side chains of MG-0.5 in D_2O ($C_{\text{MG}} = 0.05$ wt %), determined at 53 °C. The solid line stands for the fit of the experimental data using the sum of two exponential relaxation components.

441

442

443 The segmental dynamics of the PEG chains within the shell surrounding the NiPAM-rich
 444 globules should be somehow similar to the behavior of PEG chains in block copolymer
 445 micelles formed in water. One may thus compare our NMR data to the ones reported by de
 446 Graaf et al. for PNiPAM-*b*-PEG diblock copolymers, with a similar molar mass for the PEG
 447 chains (about 2000 g/mol).³⁹ In this reference, the ^1H NMR transverse relaxation signal of the
 448 PEG chains in the PNiPAM-*b*-PEG diblock micelles was reported above the VPT. The data
 449 could also be described using two $T_2(^1\text{H})$ relaxation components and the corresponding
 450 relaxation time values, $T_{2\text{S}}$ and $T_{2\text{L}}$, were found to be close to 60 ms and 1000 ms,
 451 respectively, at 45 °C and at a ^1H Larmor frequency of 500 MHz. These $T_2(^1\text{H})$ values stand
 452 in the same order of magnitude as the ones determined on MG-0.5 (70 and 780 ms). Such a
 453 similarity provides an additional support to the assignment of the fraction of mobile EG units
 454 detected above the VPTT on the ^1H NMR spectra (**Figure 7a**). Such chains should mostly
 455 correspond to dangling chains at the periphery of the NiPAM-rich globules.

456 Let us now consider the remaining fraction of the EG units in the microgels, the one that
457 becomes immobilized above the VPTT (**Figure 7b**). It may be worth remarking that such
458 frozen-like units were not detected for micelles of PNiPAM-*b*-PEG diblock copolymers.
459 Although the localization of the PEG chains at the surface of the microgel particles should be
460 favored from an enthalpic point of view, some PEG chains or PEG chain portions could
461 nevertheless be entrapped within the NiPAM globules. Indeed, as the VPTT occurs, the PEG
462 chains should diffuse toward the external part of the microgel particles. However, in contrast
463 to the case of diblock copolymers, one copolymer chain contains several PEG side chains –
464 about 12 for MG-1 for instance – so that the migration of all the PEG chains toward the
465 periphery would require a significant reorganization of the conformation displayed by the
466 copolymer chains involved within the microgel particles. Besides, during the VPTT, most of
467 the water molecules are expelled from the NiPAM-rich globules and therefore, the
468 reorientational motions of the NiPAM units undergo a significant slowing-down over the tens
469 of microseconds time scale, as evidenced in **Figure 7a**. As a result, the diffusion of the PEG
470 side chains within the forming NiPAM-rich globules is expected to become considerably
471 slower. Under this context, part of the PEG units should remain embedded within the
472 NiPAM-rich cores.

473 The NMR results derived for MG-1 were compared to the ones derived from the other
474 microgels, characterized by a varying fraction of PEG chains. In any cases (**Figure S5**,
475 Supporting Information), a similar trend is observed for $f_{\text{PEG}}(T)$. The onset of the VPTT
476 occurs at the same temperature (around 38 °C) and the transition extends over a similar
477 temperature range (from 38 to 45-47 °C). In contrast, as shown in **Figure 9**, the fraction of the
478 EG units that becomes frozen over the VPTT decreases from 66 to 15 % as the PEG content
479 within the microgel is raised up from 0.10 to 1 mol %. Such an evolution is in qualitative
480 agreement with the assignment proposed for the fraction of EG units immobilized during the

481 volume phase transition. Indeed, the increase of the proportion of PEG side chains
482 incorporated along the copolymer chains was found to result in a smaller size of the microgel
483 particles (see **Figure 3b** and **Table 2**). Therefore, as the VPTT is reached, the EG units should
484 diffuse, on average, over a larger distance to join the shell of the particles. Assuming a similar
485 kinetics for the microgel/water demixing process whatever the PEG content considered
486 between 0.10 and 1 mol %, a higher fraction of EG units should then be trapped within the
487 NiPAM-rich cores formed during the volume phase transition. This feature is in agreement
488 with the results of **Figure 9**.

489

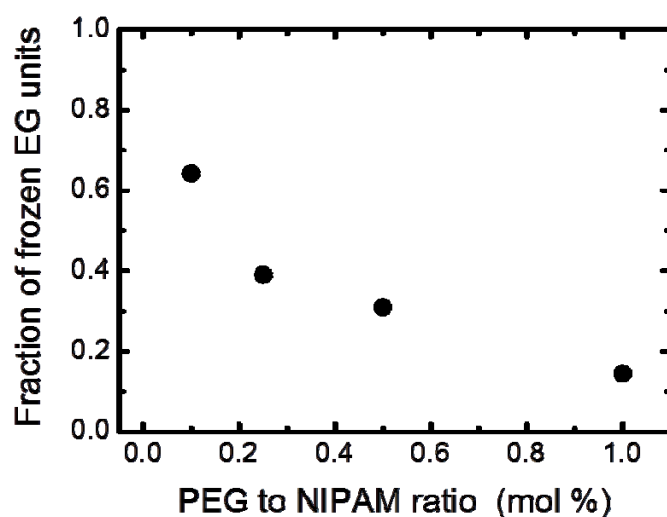


Fig. 9 Evolution of the fraction of EG units that becomes immobile, over the tens of microseconds time scale, during the volume phase separation process of the microgels, with the PEG to NiPAM molar ratio used for the microgel synthesis.

490

491

492

493

494

495

496

497

498 **CONCLUSION**

499 In the present work, we have demonstrated the possibility to easily synthesize monodisperse
500 PEGylated NiPAM-based microgels by surfactant-free precipitation polymerization. We have
501 shown that (i) the incorporation of PEG chains into the microgel synthesis allows to precise
502 control of the size and dispersity of the microgels (ii) despite the incorporation of hydrophilic
503 PEG chains, the synthesized microgels maintain a sharp VPTT similar to pure NiPAM
504 microgels thanks to the reactivity ratios of NiPAM and PEGMAOH monomers leading a
505 microgel structure in which PEG chains are located at the microgel periphery as clearly
506 shown by detailed NMR study (iii) the presence of PEG chains allows to improve the
507 colloidal stability of the microgels in electrolyte solutions even at high temperature. Finally,
508 the presence of a hydroxyl group located at the end of PEG chains allows to envisage a
509 possible post-functionalization.

510

511 **CONFLICTS ON INTEREST**

512 There are no conflicts to declare

513

514

515 **ACKNOWLEDGMENTS**

516 We gratefully acknowledge the financial support of CNRS, ESPCI, and the Ph.D. school of
517 Sorbonne Université (ED 397, Sorbonne Université) for the Ph.D. fellowship funding of J. Es
518 Sayed. The authors thank Bruno Bresson from SIMM for technical advice on scanning
519 electron microscopy. The authors gratefully acknowledge Nadège Pantoustier for fruitful
520 discussion.

521 REFERENCES

522

- 523 1 S. Nayak and L. A. Lyon, *Angewandte Chemie-International Edition*, 2005, 44, 7686-7708.
- 524 2 A. V. Kabanov and S. V. Vinogradov, *Angewandte Chemie-International Edition*, 2009, 48,
525 5418-5429.
- 526 3 J. K. Oh, R. Drumright, D. J. Siegwart and K. Matyjaszewski, *Progress in Polymer Science*,
527 2008, 33, 448-477.
- 528 4 A. E. Ekkelenkamp, M. R. Elzes, J. F. J. Engbersen and J. M. J. Paulusse, *Journal of Materials*
529 *Chemistry B*, 2018, 6, 210-235.
- 530 5 C. D. Sorrell and M. J. Serpe, *Anal. Bioanal. Chem.*, 2012, 402, 2385-2393.
- 531 6 F. A. Plamper and W. Richtering, *Accounts of Chemical Research*, 2017, 50, 131-140.
- 532 7 R. Pelton, *Advances in Colloid and Interface Science*, 2000, 85, 1-33.
- 533 8 E. Daly and B. R. Saunders, *Langmuir*, 2000, 16, 5546-5552.
- 534 9 R. H. Pelton and P. Chibante, *Colloids and Surfaces*, 1986, 20, 247-256.
- 535 10 M. J. Snowden and B. Vincent, *Journal of the Chemical Society, Chemical Communications*,
536 1992, 1103-1105.
- 537 11 Z. H. Farooqi, H. U. Khan, S. M. Shah and M. Siddiq, *Arabian Journal of Chemistry*, 2017,
538 10, 329-335.
- 539 12 M. Das, N. Sanson and E. Kumacheva, *Chemistry of Materials*, 2008, 20, 7157-7163.
- 540 13 J. S. Suk, Q. Xu, N. Kim, J. Hanes and L. M. Ensign, *Advanced Drug Delivery Reviews*, 2016,
541 99, 28-51.
- 542 14 D. Gan and L. A. Lyon, *Macromolecules*, 2002, 35, 9634-9639.
- 543 15 T. Trongsatitkul and B. M. Budhlall, *Colloids and Surfaces B-Biointerfaces*, 2013, 103, 244-
544 252.
- 545 16 N. Sanson and J. Rieger, *Polymer Chemistry*, 2010, 1, 965-977.
- 546 17 J. A. Aguilar, M. Nilsson, G. Bodenhausen and G. A. Morris, *Chemical Communications*,
547 2012, 48, 811-813.

548 18 C. Alava and B. R. Saunders, *Colloids and Surfaces A: Physicochemical and Engineering*
549 *Aspects*, 2005, 270-271, 18-25.

550 19 H. G. Schild, *Progress in Polymer Science*, 1992, 17, 163-249.

551 20 K. Otake, H. Inomata, M. Konno and S. Saito, *Macromolecules*, 1990, 23, 283-289.

552 21 H. G. Schild and D. A. Tirrell, *The Journal of Physical Chemistry*, 1990, 94, 4352-4356.

553 22 H. Chen, Q. Zhang, J. Li, Y. Ding, G. Zhang and C. Wu, *Macromolecules*, 2005, 38, 8045-
554 8050.

555 23 J. Spevacek, R. Konefal, J. Dybal, E. Cadova and J. Kovarova, *European Polymer Journal*,
556 2017, 94, 471-483.

557 24 H.-H. Lin and Y.-L. Cheng, *Macromolecules*, 2001, 34, 3710-3715.

558 25 M. Teodorescu, I. Negru, P. O. Stanescu, C. Draghici, A. Lungu and A. Sarbu, *Reactive &*
559 *Functional Polymers*, 2010, 70, 790-797.

560 26 M. Teodorescu, I. Negru, P. O. Stanescu, C. Draghici, A. Lungu and A. Sarbu, *Journal of*
561 *Macromolecular Science Part a-Pure and Applied Chemistry*, 2011, 48, 177-185.

562 27 X. Ma, J. Xi, X. Zhao and X. Tang, *Journal of polymer science part b: polymer physics*, 2005,
563 43, 3575-3583.

564 28 A. Burmistrova, M. Richter, M. Eisele, C. Üzüüm and R. von Klitzing, *Polymers*, 2011, 3,
565 1575.

566 29 M. J. Snowden, B. Z. Chowdhry, B. Vincent and G. E. Morris, *Journal of the Chemical*
567 *Society, Faraday Transactions*, 1996, 92, 5013-5016.

568 30 W. McPhee, K. C. Tam and R. Pelton, *Journal of Colloid and Interface Science*, 1993, 156,
569 24-30.

570 31 B. Wedel, T. Brändel, J. Bookhold and T. Hellweg, *ACS Omega*, 2017, 2, 84-90.

571 32 A. Pich, S. Berger, O. Ornatsky, V. Baranov and M. A. Winnik, *Colloid and Polymer Science*,
572 2009, 287, 269-275.

573 33 T. Hoare and R. Pelton, *Current Opinion in Colloid & Interface Science*, 2008, 13, 413-428.

574 34 M. Stieger, W. Richtering, J. S. Pedersen and P. Lindner, *Journal of Chemical Physics*, 2004,
575 120, 6197-6206.

576 35 X. Wu, R. H. Pelton, A. E. Hamielec, D. R. Woods and W. McPhee, *Colloid and Polymer*
577 *Science*, 1994, 272, 467-477.

578 36 R. H. Pelton, H. M. Pelton, A. Morphesis and R. L. Rowell, *Langmuir*, 1989, 5, 816-818.

579 37 A. F. Routh and B. Vincent, *Langmuir*, 2002, 18, 5366-5369.

580 38 J. Spevacek, L. Hanykova and L. Starovoytova, *Macromolecules*, 2004, 37, 7710-7718.

581 39 A. J. de Graaf, K. W. M. Boere, J. Kemmink, R. G. Fokkink, C. F. van Nostrum, D. T. S.
582 Rijkers, J. van der Gucht, H. Wienk, M. Baldus, E. Mastrobattista, T. Vermonden and W. E. Hennink,
583 *Langmuir*, 2011, 27, 9843-9848.

584

585